analytical chemistry

pubs.acs.org/ac Article

Analysis of AAV-Extracted DNA by Charge Detection Mass Spectrometry Reveals Genome Truncations

Lauren F. Barnes, Benjamin E. Draper, Justin Kurian, Yu-Ting Chen, Tatiana Shapkina, Thomas W. Powers, and Martin F. Jarrold*

Cite This: *Anal. Chem.* 2023, 95, 4310−4316 Read Online

ACCESS | Metrics & More | Article Recommendations | Supporting Information

ABSTRACT: Adeno-associated virus (AAV) is a widely used gene therapy vector. The intact packaged genome is a critical quality attribute and necessary for an effective therapeutic. In this work, charge detection mass spectrometry (CDMS) was used to measure the molecular weight (MW) distribution for the genome of interest (GOI) extracted from recombinant AAV (rAAV) vectors. The measured MWs were compared to sequence masses for a range of rAAV vectors with different GOIs, serotypes, and production methods (Sf9 and HEK293 cell lines). In most cases, the measured MWs were slightly larger than the sequence masses, a result attributed to counterions. However, in a few cases, the measured MWs were significantly smaller than the sequence masses. In these cases, genome truncation is the only reasonable explanation for the discrepancy. These results suggest that direct analysis of the extracted GOI by CDMS provides a rapid and powerful tool to evaluate genome integrity in gene therapy products.

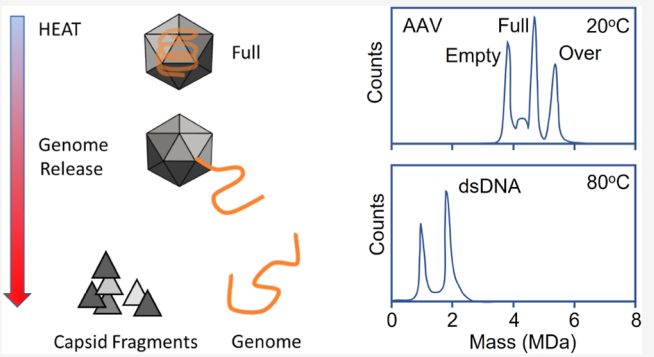

INTRODUCTION

Adeno-associated virus (AAV) is a small (26 nm), non-enveloped, icosahedral virus. Partly because of its low immunogenicity and high tissue tropism, AAV has emerged as a promising gene therapy vector.[1−4] There are currently three FDA-approved therapies in the US, with many more in clinical trials. The AAV capsid contains three viral proteins, VP1, VP2, and VP3. The sequence of VP3 is contained within VP2 along with an additional N-terminal domain. The sequence of VP2 is likewise contained within VP1. For recombinant AAV (rAAV) derived from HEK cells, the VP1-3 ratio is approximately 1:1:10.[5−7] AAV packages a single stranded (ss) DNA genome. The wild-type genome is around ∼4.7 kB in length. The genome is flanked by two inverted terminal repeats (ITRs) that play an important role in replication and genome packaging.[8−10] During preparation of recombinant vectors, plasmids provide the *Rep* and *Cap* genes that are responsible for the production of replication-assisting proteins and capsid proteins, respectively. They also provide necessary helper genes (such as those from adenovirus).

Transient transfection of adherent human HEK293 cells has been the dominant rAAV production platform used for preclinical and clinical studies to date.[11] However, manufacturing limitations with adherent HEK293 cells make it difficult to scale up the vector yield, driving up costs. Sf9 cell lines with baculovirus infection have been found to be a viable production method.[12] This method of AAV production is scalable, but there is evidence that human-cell-derived rAAVs are more potent than baculovirus-Sf9-derived vectors.[13] Some recent results point to genome truncation and ITR loss through the infection and packaging processes.[14] It has been known for some time that incomplete genomes can be packaged by both wtAAV particles and rAAV vectors, but this seems to be a particular concern with Sf9 production.[15−17]

There is a need for a quick and reliable method that can be used to ensure the integrity of the packaged genome of interest (GOI). Some truncations are too small to be reliably detected by gel-based methods. Information about genome integrity and truncation can be obtained from third-generation sequencing methods, where direct single molecule sequencing is performed with long reads.[14,18−20] However, these methods are not routine or particularly quick.

Another approach to determining whether the GOI is truncated is to measure the molecular weights (MWs) of both the empty and full particles and determine the genome MW from the difference.[17,21] However, small DNA fragments can also be packaged in both empty and full particles as well as

Received: September 26, 2022
Accepted: February 1, 2023
Published: February 22, 2023

https://doi.org/10.1021/acs.analchem.2c04234
Anal. Chem. 2023, 95, 4310−4316

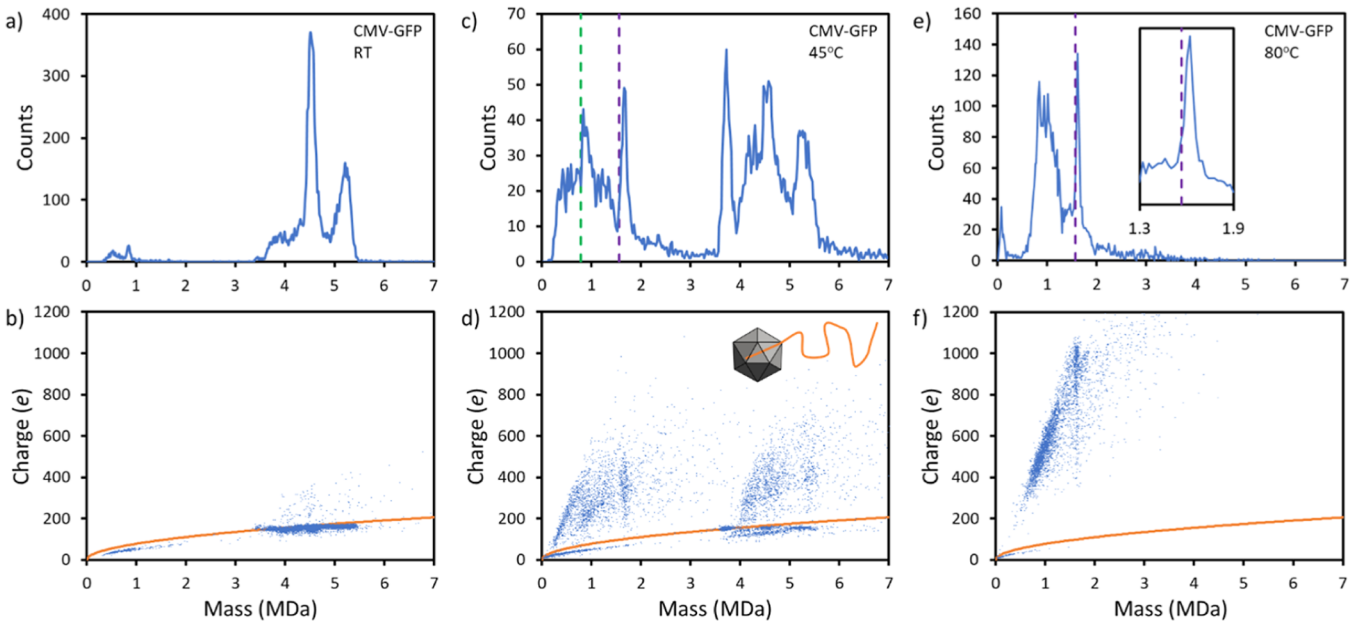

Figure 1. CDMS measurements for AAV8-CMV-GFP derived from Sf9 cells. (a,b) Mass distribution and charge vs mass scatter plot measured for an unincubated sample. The orange line in the charge vs mass scatter plots is the prediction of the Rayleigh charge limit for a spherical ion (see text). (c,d) Mass distribution and scatter plot measured after incubation at 45 °C for 15 min. The inset in (d) shows a schematic diagram of the genome extruding from the capsid. (e,f) Results after incubation at 80 °C for 15 min. The dashed green line shows the sequence mass for the released ssDNA GOI, and the dashed purple line shows the sequence mass after the complementary DNA strands base pair in solution.

heterogeneous DNA.[22−24] Incubating the AAV samples at an elevated temperature has been shown to drive out at least some of the small DNA fragments.[21] In addition, MW distributions for both the empty and full particles are broad because of heterogeneity in the number of copies of VP1-3,[25] which follow multinomial distributions.[17] Furthermore, the average VP1-3 ratios of the empty and full particles are not necessarily the same, which would compromise any measurement based on the mass difference between them.

In this work, we have extracted the DNA from the AAV vectors and directly measured the MW of the extracted DNA by charge detection mass spectrometry (CDMS). CDMS is currently used to determine empty-full ratios for AAV and to access lot-to-lot variability.[26] CDMS and AUC (analytical ultracentrifugation) provide the most reliable information about particles with masses between empty and full (i.e., particles that have packaged a partial genome).[27] While applying CDMS to determine empty-to-full ratios of intact capsids is a critical application, it is recognized that DNA can be extracted from AAV vectors by incubation at elevated temperatures. The process has been captured in AFM (atomic force microscope) images that show ssDNA extruding from heated capsids.[28,29] CDMS and Orbitrap I^2MS (a related, though lower resolution approach) have also been used to investigate the changes induced by the incubation of AAV capsids.[21,30,31] Applying CDMS to the analysis of the released DNA could enable a robust measurement of the packaged DNA, including an assessment of truncations. The measurement of MW distributions for DNA and RNA by mass spectrometry is complicated by counterions, which cause heterogeneity. The heterogeneity, in turn, limits the size of the oligonucleotides that can be measured by conventional MS.[32−34] CDMS overcomes this limitation by directly measuring the mass-to-charge ratio (m/z) and charge for each ion.[35−38] Measurements are performed for thousands of ions, and then the masses (obtained by multiplying the m/z and charge for each ion) are binned into a mass distribution.

EXPERIMENTAL SECTION

AAV Samples. AAV8, AAV9, and AAVDJ vectors generated in Sf9 cell lines were purchased from Virovek, and all had viral genome concentrations of 2×10^{13} vg/mL (viral genome per milliliter). AAV8 vectors generated in HEK293 cell lines were purchased from Vector Biolabs (AAV8-CMV-eGFP, AAV8-CMV-CRE, and AAV8-CAG-eGFP) and Vigene Biosciences (AAV8-Empty and AAV8-CMV-GFP). HEK293 vectors all had genome concentrations of 1×10^{13} genome copies per milliliter. All samples were stored at −80 °C until ready for analysis.

Incubation and DNA Extraction. AAV vectors were thawed at 4 °C prior to DNA extraction. The samples were incubated in an 80 °C water bath for 15 min before being quenched in ice water for 1 min. The samples were then exchanged into ammonium acetate solution (Honeywell 631-31-8) via Micro Bio-Spin columns (Bio-Rad, 7326221). A 10 μL aliquot was loaded onto an Advion Triversa Nanomate for electrospray.

In some cases, a second preparation method was utilized. This method required 10× dilution of 20 μL of sample with Proteinase K Buffer (Teknova, 2P0355) prior to heating the sample to 95 °C for 10 min. This step was followed by quenching in ice water for 10 min. The sample was then purified via a PureLink PCR purification kit (Invitrogen, K310001) before buffer exchange into an ammonium acetate solution, as described above. For samples where both methods were employed, the MWs of the ds GOI determined by CDMS were within the range of experimental uncertainty (RMSD ∼ 0.013 MDa).

Charge Detection Mass Spectrometry. CDMS is a single particle approach in which both the mass-to-charge ratio ($m/$

https://doi.org/10.1021/acs.analchem.2c04234
Anal. Chem. 2023, 95, 4310−4316

Table 1. AAV Samples Investigated in This Work and Comparison of the Measured dsDNA GOI Masses and Sequence Masses[a]

serotype-promotor-transgene	cell line	source	dsDNA GOI sequence mass (MDa)[b]	dsDNA GOI measured mass (MDa)	deviation (kDa)	% deviation
AAV8-CMV-CRE	Sf9	Virovek	1.367	1.38	13	1.0
AAV8-CMV-GFP	Sf9	Virovek	1.567	1.63	63	4.0
AAV8-CMV-mCherry	Sf9	Virovek	1.715	1.78	65	3.8
AAV8-CAG-GFP	Sf9	Virovek	1.771	1.73	−41	−2.3
AAV8-EF1a-GFP	Sf9	Virovek	2.130	2.08	−50	−2.3
AAV9-CMV-GFP	Sf9	Virovek	1.581	1.59	9	0.6
AAVDJ-CMV-GFP	Sf9	Virovek	1.581	1.61	29	1.8
AAV8-CAG-eGFP	HEK	Vector Biolabs	2.073	2.11	37	1.8
AAV8-CMV-CRE	HEK	Vector Biolabs	1.885	1.65	−235	−12.5
AAV8-CMV-GFP	HEK	Vigene Biosciences	1.499	1.53	31	2.1
AAV8-CMV-eGFP	HEK	Vector Biolabs	1.359	1.37	11	0.8

[a]The uncertainty in the measured masses (from multiple measurements) is ∼0.013 MDa RMSD. [b]For dsDNA with a fully ionized phosphate backbone.

z) and charge (z) are simultaneously measured for each individual ion using an electrostatic linear ion trap (ELIT). The measurements were made on a home-built instrument, which has been described elsewhere.[39−41] Briefly, ions generated by nanoelectrospray (Advion Triversa Nanomate) enter the instrument through a metal capillary and then pass through several differentially pumped regions. The first region contains a FUNPET (an ion-funnel ion-carpet hybrid),[40] followed by an RF hexapole and a segmented RF quadrupole. The FUNPET disrupts the gas jet formed by ambient gas flow through the capillary. The ions are thermalized in the hexapole, where the final ion energy is set by the dc potential on the hexapole rods. The radial distribution of the ion beam is compressed in the segmented quadrupole. Ions exiting the quadrupole are focused by an asymmetric Einzel lens into a dual hemispherical deflection energy analyzer, set to transmit ions with a narrow band of kinetic energies (centered around 100 eV/z). The transmitted ions are focused into an ELIT, where some of them are trapped and oscillate back and forth through the detection cylinder located between the endcaps of the ELIT. The oscillating ions generate a signal that is picked up by a charge sensitive amplifier. The signal is amplified and digitized and then analyzed by fast Fourier transforms (FFTs).[41] A short time window FFT is translated through the signal for each trapping event to determine whether ions are trapped for the full event. Signals for ions that do not survive for the full event are discarded. The oscillation frequency is related to the m/z, and the amplitude is proportional to the charge. Thousands of ions are measured in this way and binned into a histogram to give the mass distribution.

RESULTS AND DISCUSSION

Figure 1a shows the mass distribution measured by CDMS for AAV8-CMV-GFP prepared in Sf9 cells. The main peak at 4.5 MDa is due to rAAV that has packaged the GOI, the peak at 5.2 MDa is due to packaging of heterogeneous DNA up to the packaging capacity, and the shoulder at 3.7 MDa is due to empty particles.[20] The corresponding charge versus mass scatter plot is shown in Figure 1b. In this plot, each individual ion measurement is represented by a point. Such a plot is useful to examine the correlation between charge and mass. In this case, the charge versus mass scatter plot shows that the empty and filled capsids have very similar charges which is consistent with the DNA being packaged inside the capsids. Large ions generated by electrospray are believed to be produced by the charge residue mechanism,[42,43] where a water droplet deposits its charge on the analyte as it evaporates away. This mechanism leads to a charge that depends on the size and shape of the ion, with compact spherical geometries having smaller charges than more extended structures. Thus, for rAAV gene therapy vectors, the empty particle (a 3.7 MDa icosahedral protein shell) has an average charge of around 150 e. The full and overpackaged particles have a significantly higher mass (up to 5.4 MDa), but a similar charge because the genome is packaged inside.

Figure 1c shows the mass distribution measured after incubation of AAV8-CMV-GFP at 45 °C for 15 min. The rAAV has started to disassemble, and there is a significant population of ions with masses below 3 MDa. There is also a substantial increase in the number of empty particles at 3.7 MDa, suggesting that the genome is being released. The corresponding charge versus mass scatter plot in Figure 1d shows a substantial increase in the charges of some of the ions with masses between 4.0 and 5.5 MDa. We attribute this increase in charge to DNA extruded from the capsids, as shown in the schematic diagram inset in Figure 1d. When fully extended, the 2544 nt CMV-GFP genome is 1720 nm long—much larger than the 26 nm capsid. Therefore, when the genome extrudes from the capsid in solution, it is reasonable to expect the charge on the gas phase ion after electrospray to be significantly larger than for ions with a completely internalized genome. Note that a high charge population is not seen for the empty particles at 3.7 MDa, which is consistent with the absence of extruded genome. There are two prominent peaks in the lower mass regime. The dashed green line shows the sequence mass (the theoretical mass obtained from the sequence with a fully ionized phosphate backbone) for the ssDNA CMV-GFP GOI. Complimentary strands are packaged in AAV with equal frequency,[44] so the ssDNA can base pair in solution after it is released from the capsids. The dashed purple line shows the sequence mass for double stranded (ds) CMV-GFP GOI. The two peaks are at a slightly higher mass than the dashed lines representing the sequence masses of the ssDNA GOI and dsDNA GOI. Figure 1e shows the CDMS mass distribution measured after incubation at 80 °C for 15 min. At this temperature, the rAAV has completely disassembled. However, the peak near the expected mass of the dsDNA GOI

https://doi.org/10.1021/acs.analchem.2c04234
Anal. Chem. 2023, 95, 4310−4316

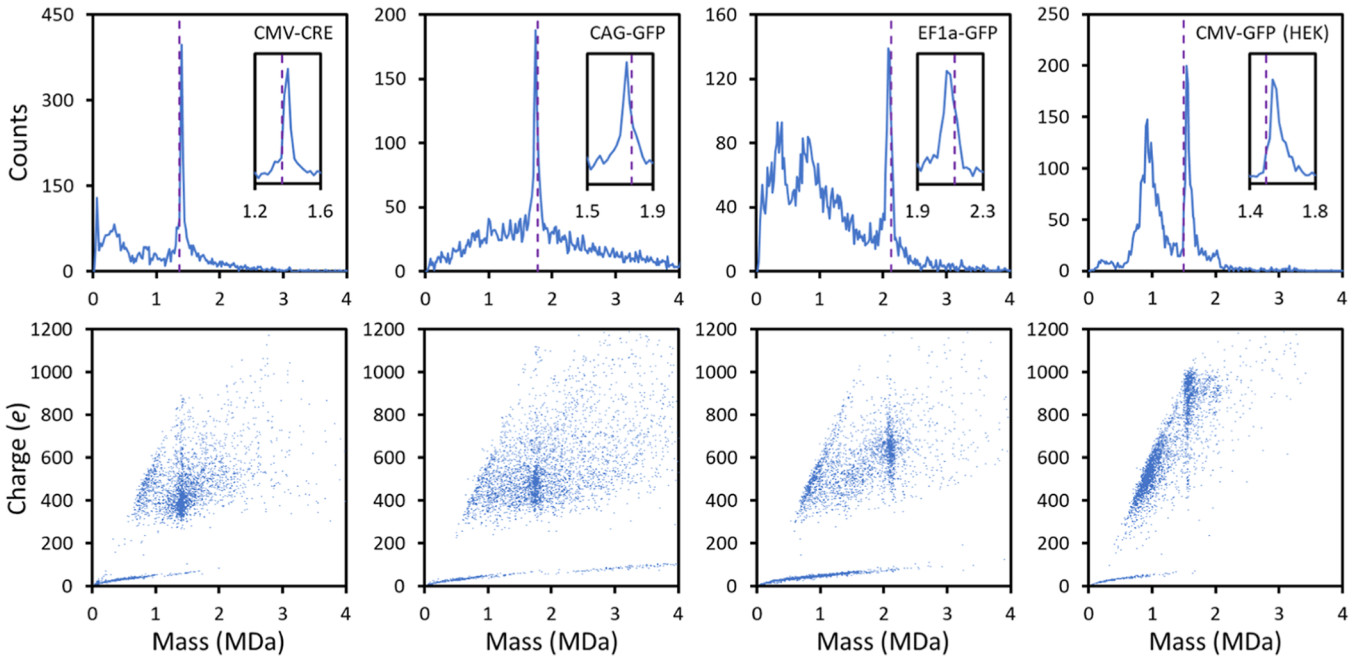

Figure 2. Representative mass distributions and charge vs mass scatter plots recorded after incubation at 80 °C for 15 min. Results are shown for AAV8-CMV-CRE, AAV8-CAG-GFP, and AAV8-EF1a-GFP derived from Sf9 cells and for AAV8-CMV-GFP derived from HEK cells. The dashed purple line shows the sequence mass for the dsDNA GOI. The insets show an expanded view of the peak attributed to the dsDNA GOI.

(dashed purple line) persists, and the peak is now sharper and closer to the dashed line indicating the sequence mass. The inset shows an expanded view of the peak. It is 55 kDa wide (FWHM). The charge versus mass scatter plot in Figure 1f shows that the sharp peak corresponds to highly charged ions with charges of around 900 e (elementary charges). The high charge is consistent with this peak resulting from dsDNA because it can adopt an elongated geometry that can accommodate much more charge than the roughly spherical rAAV vectors. As a final test, we incubated empty AAV8 particles for 15 min at 80 °C. CDMS measurements showed that they had completely disassembled, to give a broad low mass distribution (see Figure S1 in Supporting Information). They did not show a sharp peak attributable to dsDNA like that evident in Figure 1f.

Table 1 gives a list of the serotype, promotor, and transgene for the AAV samples that we investigated in this work. The table also includes the cell lines used for production, the GOI lengths, and the dsDNA GOI sequence masses. Figure 2 shows a representative selection of CDMS mass distributions and charge versus mass scatter plots measured for rAAV vectors after incubation to extract the GOI. Representative mass distributions and scatter plots for samples in Table 1, which are not given in Figures 1 and 2, are provided in Figures S2 and S3 in Supporting Information The mass distributions in Figure 2 show a single sharp peak that tracks the dsDNA GOI sequence mass. The dashed purple lines show the sequence masses for each vector. The insets show expanded views of the sharp peaks. For AAV8-CMV-CRE (from Sf9 cells) and AAV8-CMV-GFP (from HEK cells) the measured peak is at a slightly higher mass than the sequence mass. On the other hand, for AAV8-CAG-GFP and AAV8-EF1a-GFP (both from Sf9 cells) the measured peak is at a slightly lower mass than the sequence mass. The DNA masses were determined from the peaks using Gaussian fits. The average measured masses for the dsDNA GOIs are given in Table 1, where they are compared with the sequence masses. The charge versus mass scatter plots show clusters of highly charged ions at masses corresponding to the peaks in the mass distributions. Note that the average charges vary significantly from around 400 e for AAV8-CMV-CRE and AAV8-CAG-GFP (from Sf9 cells) to around 900 e for AAV8-CMV-GFP (from HEK cells). The difference in average charges probably reflects the overall geometries of the dsDNA with the more highly charged GOIs having more extended structures.[45]

Figure 3a shows a bar chart of the deviations of the measured dsDNA GOI MWs from the sequence masses for the AAV samples listed in Table 1. Numerical values for the deviations and percentage deviations are given in the last two columns of Table 1. The sample set investigated here includes a variety of GOIs for AAV8 and other serotypes prepared in HEK and Sf9 cells. For most of the AAV samples investigated, the measured dsDNA GOI MW is larger than the sequence mass. This deviation can be accounted for by counterions, which are known to contribute to the MW of DNA samples measured by mass spectrometry.[32−37] DNA is negatively charged in neutral solution because some of its backbone phosphates are ionized (the pK_a is ∼1 for isolated backbone phosphates). The dsDNA GOIs have 2219−3443 base pairs, so they have potentially up to 4438−6886 counterions. The most likely counterion is NH_4^+ because the sample is electrosprayed from an ammonium acetate solution. If all the dsDNA GOI backbone phosphates are ionized and have NH_4^+ counterions, the additional mass (beyond the fully ionized sequence mass) would be 80−124 kDa. In addition, the ds GOI ions are highly charged, with around 400 to 900 charges depending on the sample. The overall charge could be due to protonation of the DNA bases or due to the attachment of cations (presumably NH_4^+). Taking everything into account, the additional mass due to the overall charge and counterions is expected to range from 5−8 to 93−146 kDa, depending on the GOI length and overall charge. A percentage of the

https://doi.org/10.1021/acs.analchem.2c04234
Anal. Chem. 2023, 95, 4310−4316

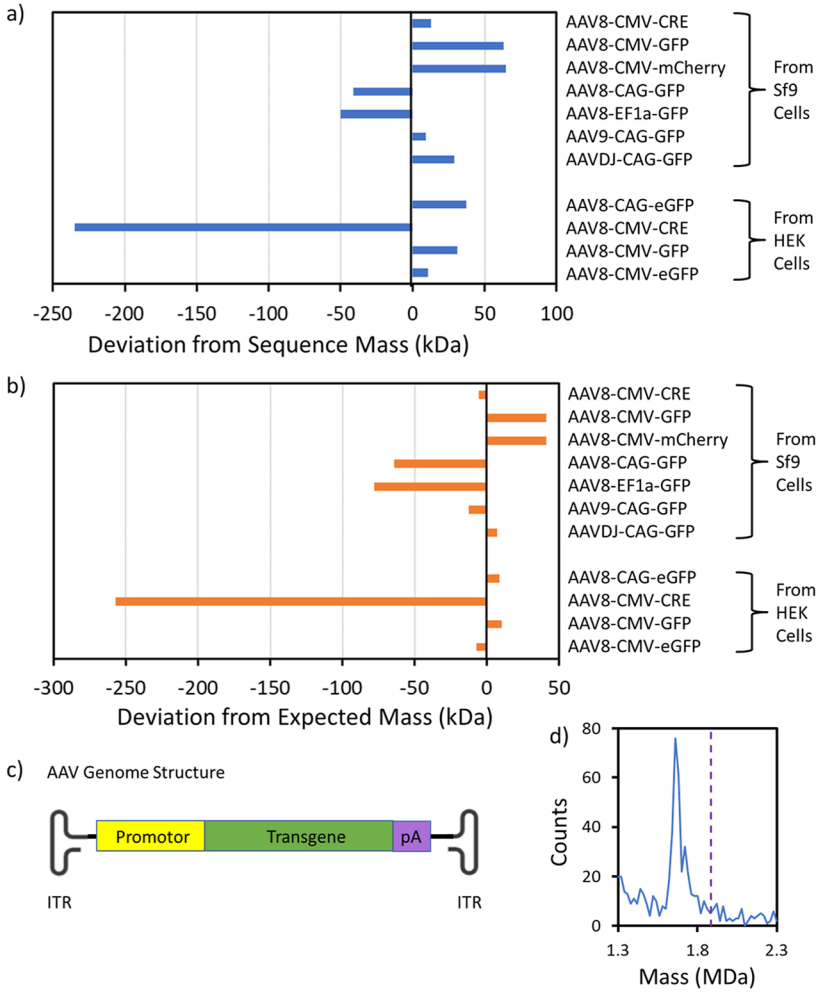

Figure 3. Summary of dsDNA mass measurements for AAV8, AAV9, and AAVDJ serotypes with a range of GOIs, derived from both Sf9 and HEK cells. (a) Bar diagram of the deviations of the measured masses from the sequence masses. (b) Bar diagram of the deviations of the measured masses from the expected masses, accounting for counterions (see text). (c) Schematic of the AAV genome structure. (d) Expanded view of the peak attributed to the dsDNA GOI from AAV8-CMV-CRE from HEK cells.

additional mass is expected to lie between 0.4 and 7−8% (with the 8% value possible when the DNA is highly charged). The differences between the measured masses and the sequence masses (for the cases in Figure 3 and Table 1, where the measured mass is greater than the sequence mass) all fall on the lower end of the expected range, indicating that the number of cations attached either as counterions or to provide the overall charge is relatively low. On the other hand, the range of positive deviations is fairly large, from 0.6 to 4.0%. In recent studies of several DNA plasmids (that will be reported elsewhere), the mass measured by CDMS was around 1% larger than the sequence mass (the deviation again being attributed to counterions). Only three of the entries in Table 1 are around +1%. Another three have deviations around +2%, while two have deviations of around +4%. Considering the uncertainty in the measurements, the difference between +1% and +2% is not particularly significant, and if we average these 6 values together, the average and RMSD are 1.3 and 0.6%. These values are not much different from the values obtained for the DNA plasmids, and this leaves two outliers (the ones with deviations of around 4%). If 1.3% of the measured mass is subtracted from the mass deviations in Table 1, the result is the deviation from the expected mass where the additional mass due to the counterions has been included. The results are shown as a bar diagram in Figure 3b. More than half of the samples in Figure 3b have deviations close to zero. In two cases (AAV8-CMV-GFP and AAV8-CMV-mCherry from Sf9 cells), the deviations are positive, and the measured masses are in both cases 41 kDa larger than the expected masses. It is not clear if the deviations could be due to genomes that are longer than expected, but in cases where the measured mass is larger than the expected mass, we cannot rule out the possibility that the extra mass is due to the adduction of other species possibly derived from the disassembled AAV particle.

There are three examples in Figure 3a, where the measured mass is less than the sequence mass. This discrepancy cannot be accounted for by counterions and indicates that the packaged genome is truncated. Figure 3c shows a schematic of the AAV genome, showing the ITRs at both ends of the ssDNA genome. As noted above, some recent results suggest that ITR loss is a concern for rAAV generated in Sf9 cells.[14] The ITRs are 145 nt long. Using the average mass for a DNA nucleotide (303.7 Da) yields an expected mass for an ITR of around 44 kDa. AAV8-CAG-GFP and AAV8-EF1a-GFP in Figure 3b have masses that are 64 and 78 kDa lower than the expected masses, respectively. However, recall that this is for dsDNA, so the average mass lost per DNA strand is 32 and 39 kDa, or in terms of DNA bases, 105 and 128 nt, respectively.

https://doi.org/10.1021/acs.analchem.2c04234
Anal. Chem. 2023, 95, 4310−4316

These values are less than expected for an ITR (45 kDa or 145 nt).

The largest deviation between the measured mass and the expected mass found in this work occurred for an AAV8-CMV-CRE sample derived from HEK cells (see Figure 3b). In this case, the deviation from the expected mass (including counterions) is 257 kDa for dsDNA or an average of 129 kDa (or 425 nt) for single strands. Figure 3d shows an expanded view of the DNA peak measured for this sample. The peak width can provide information about the distribution of truncations. If all the DNA strands had lost 425 nt, the peak would be narrow. On the other hand, a broad peak would result if there was a broad distribution in the length truncated. The peak in Figure 3d is relatively narrow, suggesting a narrow distribution. There is a high mass tail, which may indicate that some genomes are truncated by less than 425 nt.

Another way to determine the genome mass is from the difference between the masses of the empty and full particles (see ref 21). As noted in the Introduction, there are several issues with this approach. Small DNA fragments are packaged in both the empty and full particles. Although some can be removed by incubation at elevated temperatures, it is difficult to know if they have all been removed. In addition, the DNA mass determined from the full mass minus the empty mass is obtained from the difference between two large numbers, so the values should be intrinsically less reliable than those obtained directly from measuring the mass of the DNA. There is some overlap between the samples studied here and those studied in our previous work in ref 21. AAV samples studied previously were obtained from Sf9 cells, and the two particles from Sf9 cells that were identified here as having truncated genomes (AAV8-CAG-GFP and AAV8-EF1a-GFP) do have genome masses (from the difference between the empty and full masses) that are around 40 kDa smaller than expected.

CONCLUSIONS

Confirmation that the full length GOI is packaged is important because delivery of a truncated genome could substantially impair the therapeutic benefit and could cause an enhanced immune response. In this work, we have explored the idea of using CDMS measurements of the released genome to determine whether the packaged GOI in AAV gene therapy products is truncated. The CDMS approach described here uses a small sample size (10 μL) and requires around an hour to perform. We investigated 11 samples, mainly AAV8, with a range of different genomes derived from both HEK and Sf9 cells. Of the eleven samples, three showed evidence of significant truncations. Two samples derived from Sf9 cells had truncations with average single-strand deficits of around 32 and 39 kDa from the expected mass after counterions were considered. One of the samples derived from HEK cells showed a much larger average deficit of 129 kDa (after counterions were considered). Studies of a larger sample set are needed to determine the frequency of truncations, particularly the larger ones. Measurements to investigate lot-to-lot variability should also be performed. In the future, high-resolution measurements should allow the distribution of dsDNA lengths to be determined. Finally, it would be instructive to compare the CDMS measurements of genome truncation with information from third-generation sequencing methods.[18,19,23] Although a CDMS measurement can tell whether the genome is truncated and the amount that is missing, it cannot determine where the truncation occurs. Information about where the truncation occurs can be obtained from third-generation sequencing, and this information can in turn provide insight into its mechanism. Thus, the CDMS measurements of the entire genome MW and third-generation sequencing are complementary. The CDMS measurements could be used as a screen to identify truncated genomes for subsequent in depth analysis by third-generation sequencing.

ASSOCIATED CONTENT

Supporting Information

The Supporting Information is available free of charge at https://pubs.acs.org/doi/10.1021/acs.analchem.2c04234.

Mass distributions and charge versus mass scatter plots for AAV8 empty and for vectors not shown in the manuscript (PDF)

AUTHOR INFORMATION

Corresponding Author

Martin F. Jarrold − *Chemistry Department, Indiana University, Bloomington, Indiana 47405, United States;* orcid.org/0000-0001-7084-176X; Email: mfj@iu.edu

Authors

Lauren F. Barnes − *Chemistry Department, Indiana University, Bloomington, Indiana 47405, United States*

Benjamin E. Draper − *Chemistry Department, Indiana University, Bloomington, Indiana 47405, United States*

Justin Kurian − *Analytical Research and Development, Pfizer Inc., Chesterfield, Missouri 63017, United States*

Yu-Ting Chen − *Analytical Research and Development, Pfizer Inc., Chesterfield, Missouri 63017, United States*

Tatiana Shapkina − *Analytical Research and Development, Pfizer Inc., Chesterfield, Missouri 63017, United States*

Thomas W. Powers − *Analytical Research and Development, Pfizer Inc., Chesterfield, Missouri 63017, United States*

Complete contact information is available at: https://pubs.acs.org/10.1021/acs.analchem.2c04234

Notes

The authors declare the following competing financial interest(s): Two of the authors (BED and MFJ) are shareholders in Megadalton Solutions, a company that is engaged in commercializing CDMS.

ACKNOWLEDGMENTS

The research reported here was supported by a grant from Pfizer, Inc. to Indiana University.

REFERENCES

(1) Hastie, E.; Samulski, R. J. *Hum. Gene Ther.* **2015**, *26*, 257−265.

(2) Naso, M.; Tomkowicz, B.; Perry, W.; Strohl, W. *BioDrugs* **2017**, *31*, 317−334.

(3) Wang, D.; Tai, P. W. L.; Gao, G. *Nat. Rev. Drug Discovery* **2019**, *18*, 358−378.

(4) Keeler, A. M.; Flotte, T. R. *Annu. Rev. Virol.* **2019**, *6*, 601−621.

(5) Kronenberg, S.; Kleinschmidt, J. A. B.; Böttcher, B. *EMBO Rep.* **2001**, *2*, 997−1002.

(6) Kaludov, N.; Padron, E.; Govindasamy, L.; McKenna, R.; Chiorini, J. A.; Agbandje-McKenna, M. *Virology* **2003**, *306*, 1−6.

(7) Nam, H.; Lane, M.; Padron, E.; Gurda, B.; McKenna, R.; Kohlbrenner, E.; Aslanidi, G.; Byrne, B.; Muzyczka, N.; Zolotukhin, S.; Agbandje-McKenna, M. *J. Virol.* **2007**, *81*, 12260−12271.

(8) Wang Y, C.; Wang L, Y.; Aslanidi GV, Y.; Wang, L.; Jayandharan, G. R.; Aslanidi, G. V.; Li, B.; Cheng, B.; Ma, W.; Lentz, T.; Ling, C.; Xiao, X.; Samulski, R. J.; Muzyczka, N.; Srivastava, A. *J. Mol. Genet. Med.* **2015**, *09*, 1000175.
(9) Bennett, A.; Mietzsch, M.; Agbandje-McKenna, M. *Future Virol.* **2017**, *12*, 283−297.
(10) Berns, K. I. *Hum. Gene Ther.* **2020**, *31*, 518−523.
(11) Grimm, D.; Kern, A.; Rittner, K.; Kleinschmidt, J. A. *Hum. Gene Ther.* **1998**, *9*, 2745−2760.
(12) Urabe, M.; Ding, C.; Kotin, R. *Hum. Gene Ther.* **2002**, *13*, 1935−1943.
(13) Rumachik, N. G.; Malaker, S. A.; Poweleit, N.; Maynard, L. H.; Adams, C. M.; Leib, R. D.; Cirolia, G.; Thomas, D.; Stamnes, S.; Holt, K.; Sinn, P.; May, A. P.; Paulk, N. K. *Mol. Ther.—Methods Clin. Dev.* **2020**, *18*, 98−118.
(14) Tran, N. T.; Lecomte, E.; Saleun, S.; Namkung, S.; Robin, C.; Weber, K.; Devine, E.; Blouin, V.; Adjali, O.; Ayuso, E.; Gao, G.; Penaud-Budloo, M.; Tai, P. W. L. *Hum. Gene Ther.* **2022**, *33*, 371−388.
(15) Hauswirth, W. W.; Berns, K. I. *Virology* **1979**, *93*, 57−68.
(16) Laughlin, C. A.; Myers, M. W.; Risin, D. L.; Carter, B. J. *Virology* **1979**, *94*, 162−174.
(17) Pierson, E. E.; Keifer, D. Z.; Asokan, A.; Jarrold, M. F. *Anal. Chem.* **2016**, *88*, 6718−6725.
(18) Thompson, J. F.; Milos, P. M. *Genome Biol.* **2011**, *12*, 217.
(19) Dorado, G.; Gálvez, S.; Rosales, T. E.; Vásquez, V. F.; Hernández, P. *Biomolecules* **2021**, *11*, 1111.
(20) Tran, N. T.; Heiner, C.; Weber, K.; Weiand, M.; Wilmot, D.; Xie, J.; Wang, D.; Brown, A.; Manokaran, S.; Su, Q.; Zapp, M. L.; Gao, G.; Tai, P. W. L. *Mol. Ther.—Methods Clin. Dev.* **2020**, *18*, 639−651.
(21) Barnes, L. F.; Draper, B. E.; Chen, Y.; Powers, T. W.; Jarrold, M. F. *Mol. Ther.—Methods Clin. Dev.* **2021**, *23*, 87−97.
(22) Smith, P. H.; Wright, J. F.; Qu, G.; Patarroyo-White, S.; Parker, A.; Sommer, J. M. *Mol. Ther.* **2003**, *7*, S348.
(23) Chadeuf, G.; Ciron, C.; Moullier, P.; Salvetti, A. *Mol. Ther.* **2005**, *12*, 744−753.
(24) Lecomte, E.; Tournaire, B.; Cogné, B.; Dupont, J.-B.; Lindenbaum, P.; Martin-Fontaine, M.; Broucque, F.; Robin, C.; Hebben, M.; Merten, O.-W.; Blouin, V.; François, A.; Redon, R.; Moullier, P.; Léger, A. *Mol. Ther.—Nucleic Acids* **2015**, *4*, No. e260.
(25) Snijder, J.; van de Waterbeemd, M.; Damoc, E.; Denisov, E.; Grinfeld, D.; Bennett, A.; Agbandje-McKenna, M.; Makarov, A.; Heck, A. J. R. *J. Am. Chem. Soc.* **2014**, *136*, 7295−7299.
(26) O'Connor, D. M.; Lutomski, C. A.; Jarrold, M. F.; Boulis, N. M.; Donsante, A. *Hum. Gene Ther: Methods.* **2019**, *30*, 214−225.
(27) Werle, A.; Powers, T.; Zobel, J.; Wappelhorst, C.; Jarrold, M.; Lyktey, N.; Sloan, C.; Wolf, A.; Adams-Hall, S.; Baldus, P.; Runnels, H. *Mol. Ther.—Methods Clin. Dev.* **2021**, *23*, 254−262.
(28) Horowitz, E. D.; Rahman, K. S.; Bower, B. D.; Dismuke, D. J.; Falvo, M. R.; Griffith, J. D.; Harvey, S. C.; Asokan, A. *J. Virol.* **2013**, *87*, 2994−3002.
(29) Bernaud, J.; Rossi, A.; Fis, A.; Gardette, L.; Aillot, L.; Büning, H.; Castelnovo, M.; Salvetti, A.; Faivre-Moskalenko, C. *J. Biol. Phys.* **2018**, *44*, 181−194.
(30) Kostelic, M. M.; Ryan, J. P.; Brown, L. S.; Jackson, T. W.; Hsieh, C.-C.; Zak, C. K.; Sanders, H. M.; Liu, Y.; Chen, V. S.; Byrne, M.; Aspinwall, C. A.; Baker, E. S.; Marty, M. T. *Anal. Chem.* **2022**, *94*, 11723−11727.
(31) Barnes, L. F.; Draper, B. E.; Jarrold, M. F. *Mol. Ther.—Methods Clin. Dev.* **2022**, *27*, 327−336.
(32) Covey, T. R.; Bonner, R. F.; Shushan, B. I.; Henion, J.; Boyd, R. K. *Rapid Commun. Mass Spectrom.* **1988**, *2*, 249−256.
(33) Muddiman, D. C.; Smith, R. D. *Rev. Anal. Chem.* **1998**, *17*, 1−68.
(34) Sannes-Lowery, K.; Mack, D.; Hu, P.; Mei, H.; Loo, J. *J. Am. Soc. Mass Spectrom.* **1997**, *8*, 90−95.
(35) Fuerstenau, S. D.; Benner, W. H. *Rapid Commun. Mass Spectrom.* **19951995**, *9*, 1528−1538.
(36) Schultz, J. C.; Hack, C. A.; Benner, W. H. *J. Am. Soc. Mass Spectrom.* **1998**, *9*, 305−313.
(37) Schultz, J. C.; Hack, C. A.; Benner, W. H. *Rapid Commun. Mass Spectrom.* **1999**, *13*, 15−20.
(38) Halim, M. A.; Bertorelle, F.; Doussineau, T.; Antoine, R. *Rapid Commun. Mass Spectrom.* **2019**, *33*, 35−39.
(39) Contino, N. C.; Jarrold, M. F. *Int. J. Mass Spectrom.* **2013**, *345-347*, 153−159.
(40) Draper, B. E.; Anthony, S. N.; Jarrold, M. F. *J. Am. Soc. Mass Spectrom.* **2018**, *29*, 2160−2172.
(41) Draper, B. E.; Jarrold, M. F. *J. Am. Soc. Mass Spectrom.* **2019**, *30*, 898−904.
(42) Fernandez de la Mora, J. *Anal. Chim. Acta* **2000**, *406*, 93−104.
(43) Konermann, L.; Ahadi, E.; Rodriguez, A. D.; Vahidi, S. *Anal. Chem.* **2013**, *85*, 2−9.
(44) Berns, K. I.; Rose, J. A. *J. Virol.* **1970**, *5*, 693−699.
(45) Cebrián, J.; Kadomatsu-Hermosa, M. J.; Castán, A.; Martínez, V.; Parra, C.; Fernández-Nestosa, M. J.; Schaerer, C.; Martínez-Robles, M.-L.; Hernández, P.; Krimer, D. B.; Stasiak, A.; Schvartzman, J. B. *Nucleic Acids Res.* **2015**, *43*, No. e24.

https://doi.org/10.1021/acs.analchem.2c04234
Anal. Chem. 2023, 95, 4310−4316